Direct Kinetics Study of CH_2OO + Methyl Vinyl Ketone and CH_2OO + Methacrolein Reactions and an Upper Limit Determination for CH_2OO + CO Reaction

Arkke J. Eskola,[1,2] Malte Döntgen,[2] Brandon Rotavera,[1†] Rebecca L. Caravan,[1] Oliver Welz,[1‡] John D. Savee,[1§] David L. Osborn,[1] Dudley E. Shallcross,[3] Carl J. Percival,[4¥] and Craig A. Taatjes[1]**

[1]*Combustion Research Facility, Sandia National Laboratories, 7011 East Avenue, MS 9055, Livermore, California 94551, USA*

[2]*University of Helsinki, Department of Chemistry, A.I. Virtasen Aukio 1, FI-00560 Helsinki, Finland*

[3] *School of Chemistry, The University of Bristol, Cantock's Close BS8 1TS, UK*

[4]*The School of Earth, Atmospheric and Environmental Science, The University of Manchester, Simon Building, Brunswick Street, Manchester, M13 9PL, UK*

† Present address: Department of Chemistry and College of Engineering, University of Georgia, Athens, GA, 30602, USA

‡ Present address: BASF, Carl-Bosch-Str. 38, 67056 Ludwigshafen, Germany

§ Present address: ABB, 3055 Orchard Dr., San Jose, CA 95134

¥ Present address: Jet Propulsion Laboratory, 4800 Oak Grove Drive, Pasadena, CA 91109 USA

* Corresponding authors: arkke.eskola@helsinki.fi, cataatj@sandia.gov

Abstract

Methyl vinyl ketone (MVK) and methacrolein (MACR) are important intermediate products in atmospheric degradation of volatile organic compounds, especially of isoprene. This work investigates the reactions of the smallest Criegee intermediate, CH_2OO, with its co-products from isoprene ozonolysis, MVK and MACR, using multiplexed photoionization mass spectrometry (MPIMS), with either tunable synchrotron radiation from the Advanced Light Source or Lyman-α (10.2 eV) radiation for photoionization. CH_2OO was produced via pulsed laser photolysis of CH_2I_2 in the presence of excess O_2. Time-resolved measurements of reactant disappearance and of product formation were performed to monitor reaction progress; first order rate coefficients were obtained from exponential fits to the CH_2OO decays. The bimolecular reaction rate coefficients at 300 K and 4 Torr are $k(CH_2OO + MVK) = (5.0 \pm 0.4) \times 10^{-13}$ cm^3 s^{-1} and $k(CH_2OO + MACR) = (4.4 \pm 1.0) \times 10^{-13}$ cm^3 s^{-1}, where the stated ± 2σ uncertainties are statistical uncertainties. Adduct formation is observed for both reactions and is attributed to the formation of secondary ozonides (1,2,4-trioxolanes), supported by master equation calculations of the kinetics and the agreement between measured and calculated adiabatic ionization energies. Kinetics measurements were also performed for a possible bimolecular $CH_2OO + CO$ reaction and for the reaction of CH_2OO with CF_3CHCH_2 at 300 K and 4 Torr. For $CH_2OO + CO$, no reaction is observed and an upper limit is determined: $k(CH_2OO + CO) < 2 \times 10^{-16}$ cm^3 s^{-1}. For $CH_2OO + CF_3CHCH_2$, an upper limit of $k(CH_2OO + CF_3CHCH_2) < 2 \times 10^{-14}$ cm^3 s^{-1} is obtained.

1. Introduction

Carbonyl oxides, also known as Criegee intermediates (CIs), are formed from the ozonolysis of alkenes and play an important role in tropospheric chemistry.[1] Reaction of ozone (O_3) with alkenes is initiated by formation of a primary ozonide (POZ) in the 1,3-cycloaddition reaction between ozone and alkenes.[2] Subsequent, rapid decomposition of the highly excited POZ (addition of ozone is exothermic by $\geq$ 50 kcal mol^{-1})[3] leads to formation of CI and a carbonyl compound (aldehyde or ketone). The CI formed from the decomposition of the POZ contains significant internal energy and can isomerize further or dissociate.[3] However, a significant fraction of nascent CI is stabilized in non-reactive collisions with atmospheric constituents, mainly with N_2. These stabilized Criegee intermediates (sCIs) are highly reactive and the understanding of their possible impact on tropospheric chemistry[4] has increased since the discovery of a method to produce sCIs for kinetics studies, which employs photolysis of the corresponding *gem* di-iodoalkane compound in the presence of O_2.[5] For example, photolysis of CH_2I_2 produces CH_2I radical and in presence of O_2 the subsequent $CH_2I + O_2 \rightarrow CH_2OO + I$ reaction produces the smallest sCI, CH_2OO, with almost unity yield at low (~ 4 Torr) pressure.[5-8]

Methyl vinyl ketone (MVK, $CH_3C(O)CHCH_2$) and methacrolein (MACR, $CH_2C(CH_3)CHO$), see Scheme 1, are among the main products in OH-initiated oxidation of isoprene in presence of NO_x as well as in ozonolysis of isoprene. Under high-NO_x conditions the combined yield of MVK and MACR from OH-initiated oxidation of isoprene is in the range 54-72 %,[9-11] while under low-NO_x or NO_x-free conditions the combined yield is suppressed.[12] In isoprene ozonolysis the combined yield of MVK and MACR is about 50 – 55 % and has been shown to increase under humid conditions by approximately 13 %.[13-15]

A secondary ozonide (SOZ) is formed in a 1,3-bipolar cycloaddition reaction of an sCI with an aldehyde or a ketone. SOZs have 1,2,4-trioxolane structure and were first observed in liquid-phase ozonolysis of alkenes.[2, 16] In liquid-phase ozonolysis SOZs are prominent partly because the cage-effect of a liquid promotes the sCI to recombine with its carbonyl compound co-product and produce an SOZ.[2, 16] In the gas-phase, where this cage effect does not exist, sCIs are consequently more likely to react with other compounds than with the conjugate carbonyl compound. However, SOZs are also formed in the gas phase and have been observed in indirect ozonolysis experiments[17, 18] and more recently in direct kinetics measurements[19] of CH_2OO with acetone and hexafluoroacetone.

In this work we investigate kinetics of the following reactions:

$$CH_2OO + CH_3C(O)CHCH_2 \qquad (R1)$$

$$CH_2OO + CH_2C(CH_3)CHO \qquad (R2)$$

and probe possible product species at 300 K and 4 Torr. In addition, upper limits are determined for the rate coefficients of the bimolecular reactions

$$CH_2OO + CO \qquad (R3)$$

$$CH_2OO + CF_3CH{=}CH_2 \qquad (R4)$$

at 300 K and 4 Torr. The current work provides the first direct kinetics experiments on these reactions.

2. Experiment

Experiments were performed using a time-resolved, multiplexed photoionization (time-of-flight) mass spectrometry (MPIMS)[20] apparatus employing either tunable synchrotron radiation from the Advanced Light Source (ALS) or Lyman-α (10.2 eV) radiation from a hydrogen discharge lamp for photoionization. The apparatus consists of a halocarbon-wax coated quartz reactor with an inner diameter of 1.05 cm coupled to the MPIMS. Pulsed excimer laser photolysis (4 or 10 Hz repetition rate, 248 nm) of CH_2I_2 precursor generated CH_2I radicals whose subsequent, rapid reaction with O_2 ($k' \sim 20000\ s^{-1}$) produced a nearly uniform CH_2OO concentration in the reactor according to the reaction $CH_2I + O_2 \rightarrow CH_2OO + I$. The reacting mixture was continuously sampled through a ~ 0.65 mm diameter orifice in the sidewall of the reactor. Typical concentrations were $[MVK]_{max} \approx [MACR]_{max} \sim 2 \times 10^{15}$ cm^{-3}, $[CH_2I_2] \sim 1.5 \times 10^{13}$ cm^{-3}, $[O_2] \sim 1 \times 10^{16}$ cm^{-3}, with helium added to a total pressure of 4 Torr. Relatively high reactant concentrations were used in upper limit determinations for the CH_2OO + CO and $CH_2OO + CF_3CHCH_2$ reactions ($[CO]_{max} \sim 4 \times 10^{16}$ cm^{-3}, $[CF_3CHCH_2]_{max} \sim 8 \times 10^{15}$ cm^{-3}). Concentrations of reactants were set by controlling the mass flow of manometrically prepared gas mixtures. Photosensitive and potentially reactive metal carbonyl contaminants were removed from the CO flow[22] by using a commercial chemical sorbent purifier immediately upstream of the reactor inlet. The cross-sections at 248 nm are small enough for MVK ($\sim 2.5 \times 10^{-21}$ cm^2)[21] and MACR ($\sim 1.5 \times 10^{-21}$ cm^2),[21] that at the fluences employed (4×10^{16} cm^{-2}) less than ~ 0.01 % of the reactants absorb a photon, and the effects of photodissociation of MVK or MACR on the removal rate for CH_2OO could be neglected. Neither CO nor CF_3CHCH_2 absorbs significantly at 248 nm.

To characterize products formed in R1 and R2, full mass-, time-, and energy-resolved datasets, $I(m/z, t, E)$, were obtained by recording time-resolved mass-spectra $I(m/z, t)$ as a function of the photon energy E. Typically, the photon energy was scanned from 9.0 – 10.75 eV in steps of 25

meV and normalized to the ALS photon flux. Signal was background-corrected by subtracting the average of the pre-photolysis signal. Experiments to determine bimolecular reaction rate coefficients were carried out using ~ 10.2 eV radiation from a hydrogen discharge lamp with a MgF_2 window.

3. Computation

3.1 Adiabatic ionization energy (AIE) calculations. For the neutral molecular structures, the lowest-energy conformers were determined using one-dimensional hindered rotor scans at the HF/def2-TZVP level of theory. Based on these conformers, neutral and cationic molecular structures were geometry-optimized at the B3LYP-D3BJ /def2-TZVP level of theory[23] without additional hindered rotor scans. Using the B3LYP geometries, single-point energies were calculated at the MP2/cc-pVDZ (/cc-pVTZ) and DLPNO-CCSD(T)/cc-pVTZ (/cc-pVQZ) levels of theory.[24, 25] The DLPNO approximation of CCSD(T) was used because exact CCSD(T)/cc-pVQZ calculations would have been computationally prohibitively expensive for the CH_2OO-MVK/MACR adduct structures. Complete basis set (CBS) limits were calculated using the ECBS = (43EQZ − 33ETZ)/(43 − 33) scheme[26] for the DLPNO-CCSD(T) calculations and using the CBS* scheme proposed by Kruse et al.[27] for the combination of MP2 and DLPNO-CCSD(T) calculations. All quantum-mechanical calculations were carried with the ORCA software package.[28]

Adiabatic ionization energies (AIEs) of the CH_2OO-MVK/MACR adduct structures were calculated at the GFN-xTB,[29] HF/def2-TZVP, B3LYP-D3BJ/def2-TZVP, DLPNO-CCSD(T)/CBS(TZ,QZ), and CBS* levels of theory. The uncertainties associated with the ionization energy predictions at the different levels of theory were superficially evaluated using

a set of eight reference structures: acetone,[30] 2-butanone,[31] acetaldehyde,[32] propanal,[32] 2-methyl-propanal,[33] 2-methyl-1-propene,[34] cyclopentane,[34] and tetrahydrofuran.[35] The results (shown in Table S1) show that the DLPNO-CCSD(T)/CBS(TZ,QZ) level of theory systematically overestimates AIEs, and the B3LYP-D3BJ/def2-TZVP and CBS* levels of theory systematically underestimate AIEs. Combining these three methods compensates systematic errors and gives AIEs that are less than half as uncertain as the uncombined AIEs in terms of mean unsigned errors (MUEs): 0.09 eV vs. 0.04 eV. The combination is linear with weights calculated from the reciprocals of mean squared errors (MSEs):

$$IE_{\text{combined}} = 0.67 \times IE^{\text{CBS(TZ,QZ)}}_{\text{DLPNO-CCSD(T)}} + 0.28 \times IE^{\text{CBS}^*} + 0.05 \times IE^{\text{def2-TZVP}}_{\text{B3LYP-D3BJ}} \qquad (1)$$

The proposed combination of AIE calculations (Eqn. 1) was tested for an additional set of eight reference structures: 2-pentanone,[36] 3-pentanone,[31] butanal,[33] MVK,[37] ethene,[38] methoxyethene,[35] cyclopentane,[39] and 2,5-dihydrofuran.[40] Again, the combination scheme reduces uncertainty by about 50 % (0.09 eV vs. 0.05 eV), as can be seen in Table S2. The present training set (8 compounds), test set (8 compounds), and the variety of *ab initio* methods are not large enough to conclude that the presented combination scheme is generally applicable. For the present purpose, however, the good extrapolation behavior from the training set to the test set, in combination with the structural similarities between the 16 tested compounds and the 8 structures of adduct products of CH_2OO + MVK and CH_2OO + MACR reactions, leads to the conclusion that this scheme is well-suited to the 8 adduct structures.

3.2 Stationary point calculations and RRKM/ME simulations. In addition to the adiabatic ionization energy calculations, kinetics of the CH_2OO + MVK and CH_2OO + MACR addition reaction were calculated using Rice-Ramsperger-Kassel-Marcus (RRKM) theory / Master

Equation (ME) simulations. For each reaction channel, the reactants CH_2OO + MVK / CH_2OO + MACR, a pre-reaction van der Waals (vdW) complex, a transition state (TS) for the reaction from the vdW complex to the adduct, and the adduct were included in the ME. Formation of the VdW complex is assumed to be barrierless and was modeled *via* phase space theory,[41] using the same potential for describing relative translation for all adducts. Collisional energy transfer is modeled using an exponential-down model[42] with

$$\langle \Delta E_{down} \rangle = 200\ cm^{-1} \times (T\ /\ 300\ K)^{0.85}, \quad (2)$$

using the weak collider helium (He) as the bath gas. The Lennard-Jones (LJ) collision frequency[42] is calculated using σ = 2.55 Å and ε = 10.0 K for He.[43] For the adduct structures, LJ parameters were obtained *via* group additivity theory as implemented in the RMG[44] software package and are listed in Table S3. The RRKM/ME simulations were carried out with the MESS[45] software package.

4. Results and Discussion

4.1 Time behavior and bimolecular reaction rate coefficient determinations

Experiments were performed under pseudo-first-order conditions (*i.e.* contribution of CH_2OO + CH_2OO reaction was negligible in comparison to CH_2OO + MVK or CH_2OO + MACR reaction and [CH_2OO] << [MVK or MACR]). Signal decays could consequently be fitted using a single exponential function to obtain the pseudo-first-order rate coefficients k'(CH_2OO + MVK or MACR). Figures 1a and 2a show the measured CH_2OO decay signals in presence of MVK and MACR reactants. The fit to the data shown in figures 1a and 2a was convolved with an instrument response function.[5] Measurements were performed over a range of MVK or MACR reactant

concentrations in order to derive bimolecular reaction rate coefficients $k(CH_2OO + MVK \text{ or } MACR)$ from

$$k'(CH_2OO + MVK) = k(CH_2OO + MVK)\times[MVK] + k_{wall} \quad (3)$$

$$\text{and } k'(CH_2OO + MACR) = k(CH_2OO + MACR)\times[MACR] + k_{wall} \quad (4)$$

using linear fitting to the pseudo-first order values. The effective first order rate coefficient k_{wall} captures reaction of CH_2OO on the walls of the reactor as well as possible gas phase removal that does not depend on MVK or MACR. In the present configuration this background removal depends somewhat on the wall coating and is on the order of 100 - 200 s^{-1}. Experimental values of $k'(CH_2OO + MVK \text{ or MACR})$ *versus* [MVK or MACR] are plotted in Figure 3, which return the following bimolecular reaction rate coefficients at 300 K and 4 Torr: $k(CH_2OO + MVK) = (5.0 \pm 0.4) \times 10^{-13}$ cm^3 s^{-1} and $k(CH_2OO + MACR) = (4.4 \pm 1.0) \times 10^{-13}$ cm^3 s^{-1}, where the stated $\pm 2\sigma$ bounds reflect the uncertainty in the fit.

Bimolecular reaction rate coefficients of CH_2OO with carbonyl and alkene compounds at about 300 K from the direct kinetics measurements are compared in Table 1.[19, 46, 47] From the comparison it is apparent that carbonyl compounds are significantly (more than 100×) more reactive toward CH_2OO than alkenes. In addition, substituting methyl groups in acetone with strongly electron withdrawing CF_3 groups also significantly increases reactivity (more than 100×). The rate coefficients for CH_2OO + MVK and CH_2OO + MACR reactions are similar to each other and lie between the values for the CH_2OO + acetone and CH_2OO + acetaldehyde reactions.

Figure 4 shows a bimolecular plot of CH_2OO decay *versus* [CO] from which an upper limit $k(CH_2OO + CO) < 2 \times 10^{-16}$ cm^3 s^{-1} at 300 K temperature and 4 Torr pressure is obtained. Recent

studies[48, 49] that applied a complex kinetics model to O_3 + ethene measurements in the EUPHORE chamber suggested values of $k(CH_2OO + CO)$ from ~ 10^{-15} – 10^{-16} cm^3 s^{-1} at 300 K -- however the upper limit obtained in this study is consistent only with the lowest range of those estimates. The present relatively low upper limit value is consistent with a recent theoretical study[49] by Vereecken *et al.* where the bimolecular reaction rate coefficient of CH_2OO + CO at 298 K was calculated to be 2×10^{-21} cm^3 s^{-1}. The theoretical potential energy surface is characterized by a shallow pre-reactive complex followed by a substantial (~10 kcal mol^{-1} above energy of the reactants) reaction barrier, leading to a slow effective bimolecular rate coefficient.[49]

4.2 Addition products of reactions R1 and R2 and formation of secondary ozonides (SOZs)

Both CH_2OO + MVK (R1) and CH_2OO + MACR (R2) reactions have several possible addition products (adducts), shown in Schemes 2 and 3. The 1,3-bipolar cycloaddition reaction of an sCI with a ketone or an aldehyde can lead to the formation of a 1,2,4-trioxolane structure (SOZ), see Schemes 2c and 3g. Similarly to CH_2OO addition to a ketone or an aldehyde group, CH_2OO can also add to a C=C double bond *via* a similar 1,3-bipolar cycloaddition reaction.[46, 47, 50, 51] Product structures from CH_2OO addition to a C=C double bond of MVK and MACR are shown in Schemes 2a, 2b and 3e, 3f, which, however, are not called SOZs, because they do not have 1,2,4-trioxolane structure, but rather a 1,2-dioxolane structure. In reactions R1 and R2 formation of seven-membered ring structure addition products is also possible, see Schemes 2d and 3h.

Figures 1b and 2b show photoionization spectra of the *m*/*z* channels whose time behavior corresponds to formation of products of reactions R1 and R2, as shown in Figures 1a and 2a. Figures S2a – S2c compare signals at *m/z* = 116, 101, 84, and 43 from R1 with each other showing that all signals have the same, product-type time-behavior with respect to decay of CH_2OO

reactant, within experimental uncertainty, suggesting they originate from reaction R1. The signal of the CH_2OO-MVK adduct parent ion at *m/z* = 116 is very weak whereas signal at *m/z* = 101, probably originating from a neutral methyl loss from an ionized adduct (*i.e.* from dissociative ionization of the SOZ or one of its isomers),[19] is relatively strong. Strongest ion signals appear at *m/z* = 43, which probably originates from a dissociative ionization process, as does signal at *m/z* = 84. The (neutral) cofragments are not detected. Figure S3 compares signals at *m/z* = 116, 86, and 30 from reaction R2 with each other and again all signals have the same time-behavior, mirroring decay of CH_2OO reactant. In the case of the CH_2OO-MACR adduct, the parent mass signal at *m/z* = 116 is fairly strong. For the analogous reaction of CH_2OO with acetaldehyde, MPIMS experiments did not detect the SOZ.[19] Signals at *m/z* = 86 and 30 likely reflect dissociative ionization of the adduct, where apparently either fragment may carry the charge.

To help identify the observed adducts of reactions R1 and R2, adiabatic ionization energies (AIEs) of all potential structures of addition reaction products, shown in Schemes 2 (A – D) and 3 (E – H), were calculated. Final results of calculated AIEs of structures A – H are given in Table 2. It is clear from the AIE data that while AIEs of structures A – C and E – G are not very far from each other, calculated AIEs of structures D and H, 8.61 eV and 8.59 eV, are much lower than the observed parent ion signal onsets ($\geq$ 9.2 eV) shown in figures 1b and 2b. From this large discrepancy we conclude that structures D and H are not formed in any significant yield in the current experiments and, consequently, they are not considered further. Comparing the AIEs of structures A – C with the energy-resolved signal of *m/z* = 116 in Figure 1b, may suggest some preference to select structure C with a calculated AIE of 9.21 eV; however, the combined uncertainties in the calculated and experimental ionization energies preclude an unambiguous assignment to structure C. In the case of reaction R2, comparing the AIEs of structures E – G with

the energy-resolved signal of *m/z* = 116 in Figure 2b, best agreement is obtained with structure G (9.45 eV), although other structures have only slightly lower calculated AIEs (F at 9.29 eV and E at 9.25 eV). To summarize, comparison of the observed onsets in the photoionization energy-dependent signals corresponding to the adducts with calculated AIEs of potential adduct species is consistent with SOZ formation in both CH_2OO + MVK and CH_2OO + MACR reactions.

MVK has ketone and alkene functional groups while MACR has aldehyde and alkene functional groups, see Scheme 1. As discussed above, CH_2OO adds to a double bond *via* a 1,3-bipolar cycloaddition reaction.[46, 47, 50, 51] However, as can be seen from Table 1, CH_2OO addition to compounds with one or two C=C double bonds (which at the same time to not have a C=O functionality) is a slow reaction in comparison to addition to ketone or aldehyde group. Both MVK and MACR can be considered as substituted ethenes; MVK with a moderately electron withdrawing ketone (acetyl) group and MACR with a weakly electron donating alkyl (methyl) group and a moderately electron withdrawing aldehyde (formyl) group. More polar C=C bonds are expected to react faster with sCIs. However, even in case of CF_3CHCH_2, where the strongly electron withdrawing CF_3 group should make this double bond polar and reactive, the reaction with CH_2OO is slow. Figure S3 shows a bimolecular plot of CH_2OO decay *versus* [CF_3CHCH_2] from which an upper limit $k(CH_2OO + CF_3CHCH_2) < 1.75 \times 10^{-14}$ cm^3 s^{-1} is obtained. Consequently, ratios $k(CH_2OO + CF_3CHCH_2) / k(CH_2OO + MVK) \approx k(CH_2OO + CF_3CHCH_2) / k(CH_2OO + MACR) < 1.75 \times 10^{-14}$ cm^3 s^{-1} / 4.4×10^{-13} cm^3 s^{-1} ≈ 0.04 can be considered as an estimate of upper limit of yield of CH_2OO reaction with a double bond of MVK or MACR. This empirical approach suggests that other reaction channels, *i.e.* CH_2OO reactions with a carbonyl group (which lead to structures C and G) are more important.

Table 3 shows calculated stationary point energies on the potential energy surfaces. Compounds D and H were excluded from calculations because their calculated AIEs are in considerable disagreement with the experiments, clearly suggesting they are not formed in any appreciable yield as products of these reactions. Recent[52] and current calculations (Table 3) show that CH_2OO addition to an aldehyde is a barrierless process forming a pre-reaction van der Waals complex ~ 5 kcal mol^{-1} or more below energy of the reactants followed by a small (< 3 kcal mol^{-1}) submerged barrier leading to SOZ formation with significant (~50 kcal mol^{-1})[52] internal excitation.

Reaction of CH_2OO with an alkene also leads to a pre-reaction van der Waals complex with an energy about 3 kcal mol^{-1} or more below the energy of reactants.[51] However, the barrier between the van der Waals complex and the adduct is either above or only slightly below the energy of reactants and therefore often much higher than in the case of CH_2OO addition to an aldehyde .[51] In addition, the rate-determining transition state located on this barrier is slightly tighter than for addition to C=O, which with other factors discussed above causes the CH_2OO reaction with an alkene being in general almost two orders of magnitude slower than the CH_2OO reaction with an aldehyde.[46]

The current RRKM/ME calculations of bimolecular reaction rate coefficients to form compounds with structures C and G gives values, at 300 K and 4 Torr, of $k(CH_2OO + MVK \rightarrow SOZ) = 3.6 \times 10^{-13}$ cm^{-3} s^{-1} and $k(CH_2OO + MACR \rightarrow SOZ) = 6.6 \times 10^{-13}$ cm^{-3} s^{-1}, in reasonable agreement with the current direct kinetics measurements. SOZs are formed with significant internal excitation, which can facilitate further isomerization and decomposition reactions leading to bimolecular products, especially at low pressures as in the current experiments. The reactions are calculated to be in the fall-off region (e.g., $k(CH_2OO + MVK \rightarrow SOZ)$ is ~ 65% of the high pressure limit at 4 Torr and near 300 K), so including possible dissociation channels for the SOZ (calculation of

which is outside the scope of the present work) could slightly increase the predicted rate coefficients. Moreover, the calculated isomeric branching fractions support the inferred structures of products of addition reactions under current experimental conditions (300 K, 4 Torr): for CH_2OO + MVK calculated branching fractions are 0.03 (A), 0.09 (B), and (0.88) C, while for CH_2OO + MACR they are 0.00 (E), 0.01 (F), and 0.99 (G).

From the arguments presented above we infer that the most likely addition reaction products formed in both R1 and R2 are SOZs, structures C and G. Because of the high concentrations of MVK and MACR required to measure kinetics of R1 and R2 and their relatively low ionization energies, highest photon energies were limited to 10.75 eV to avoid extremely strong signal at *m/z* = 70 from ionization of MVK and MACR damaging the detector. This prevented detection of certain potential products with AIEs > 10.75 eV (formaldehyde, formic acid etc.).

However, the potential origin of the observed signal at *m/z* = 86 in reaction R2, see Figures 2b and S2, was investigated further. In the reaction of CH_2OO with acetaldehyde, no signal was observed at the parent mass, but acetic acid product was observed and attributed to dissociation of the (neutral) SOZ.[19] An analogous dissociation in the MACR reaction could lead to methacrylic acid (mass 86). The absolute photoionization spectrum of methacrylic acid was measured in this work (shown in Figure S4a and compared with Figure 2b signal in Figure S4b). Although there is a good agreement between the energy onset and low energy region for the spectrum of the product at *m/z* = 86 and the absolute photoionization cross-section of methacrylic acid (energies below about 10.3 eV), at higher photon energies deviation is increasingly significant, precluding assignment of *m/z* = 86 signal to methacrylic acid.

5. Conclusions

In this work bimolecular rate coefficients of CH_2OO + MVK and CH_2OO + MACR reactions as well as upper limits of CH_2OO + CO and CH_2OO + CF_3CHCH_2 reactions were determined at 300 K and 4 Torr in direct, time-resolved experiments. Although both CH_2OO + MVK and CH_2OO + MACR reactions can each lead to formation of four different adduct isomers (that is eight different isomers altogether) by CH_2OO addition to either the C=C or C=O bonds or the terminal ends of the conjugated C=C-C=O system, it is inferred in this work that the adducts formed and observed at least at the parent mass are most likely secondary ozonides formed by CH_2OO addition to the C=O bonds. The low upper limit of bimolecular rate coefficient of CH_2OO + CO suggest this reaction is not important in the troposphere.

Acknowledgments

This material is based upon work supported by the Division of Chemical Sciences, Geosciences and Biosciences (CSGB), Office of Basic Energy Sciences (BES), U.S. Department of Energy (USDOE). B.R., R.L.C., O.W., J.D.S., D.L.O., C.A.T., and the work of A.J.E. at Sandia were funded through CSGB/BES. The work of A.J.E. at the University of Helsinki analyzing data and preparing this manuscript is supported by the Academy of Finland, Grant No. 288377. Work of M.D. is supported by the Academy of Finland, Grant No. 298910. The participation of C.J.P. and D.E.S. was supported by NERC Grants NE/P013104, NE/I014381, NE/K004905. The Advanced Light Source is supported by the Director, Office of Science, BES/USDOE under Contract No. DE-AC02-05CH11231 at Lawrence Berkeley National Laboratory. Sandia National Laboratories is a multimission laboratory managed and operated by National Technology and Engineering Solutions of Sandia, LLC., a wholly owned subsidiary of Honeywell International, Inc., for the USDOE's National Nuclear Security Administration under contract DE-NA0003525. This paper describes objective technical results and analysis. Any subjective views or opinions that might be

expressed in the paper do not necessarily represent the views of the USDOE or the United States Government.

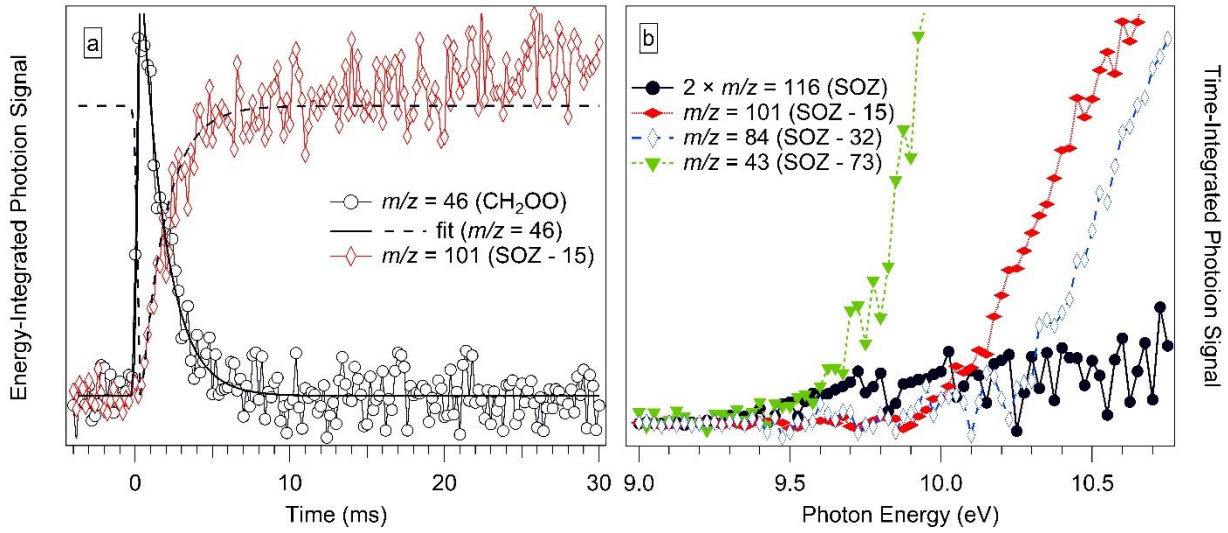

Figure 1. Experimental data from CH_2OO + $CH_3C(O)CHCH_2$ (methyl vinyl ketone, MVK) reaction measurements at 4 Torr and about 300 K. **a**) Comparison of time behaviors of CH_2OO decay (signal at *m/z* = 46) with the formation of CH_2OO-MVK adduct observed at *m/z* = 101, which is expected to originate from dissociative ionization of the adduct with parent *m/z* = 116. A single-exponential fit to the CH_2OO signal decay trace is also shown. Time-resolved signals were obtained by integration over photon energies from 9.0 – 10.75 eV. Signal intensities were arbitrarily multiplied to facilitate comparison. Product formation signal at *m/z* = 101 is compared with the weak parent signal at *m/z* = 116 in figure S2a. **b**) Comparison of energy-resolved signals with potential origin from the CH_2OO-MVK adduct. The parent mass signal at *m/z* = 116 is weak and signals at *m/z* = 101 and *m/z* = 43 are suggested to originate from dissociative ionization of the CH_2OO-MVK adduct. Time-resolved signals of product formation are compared in Figures S2a – c.

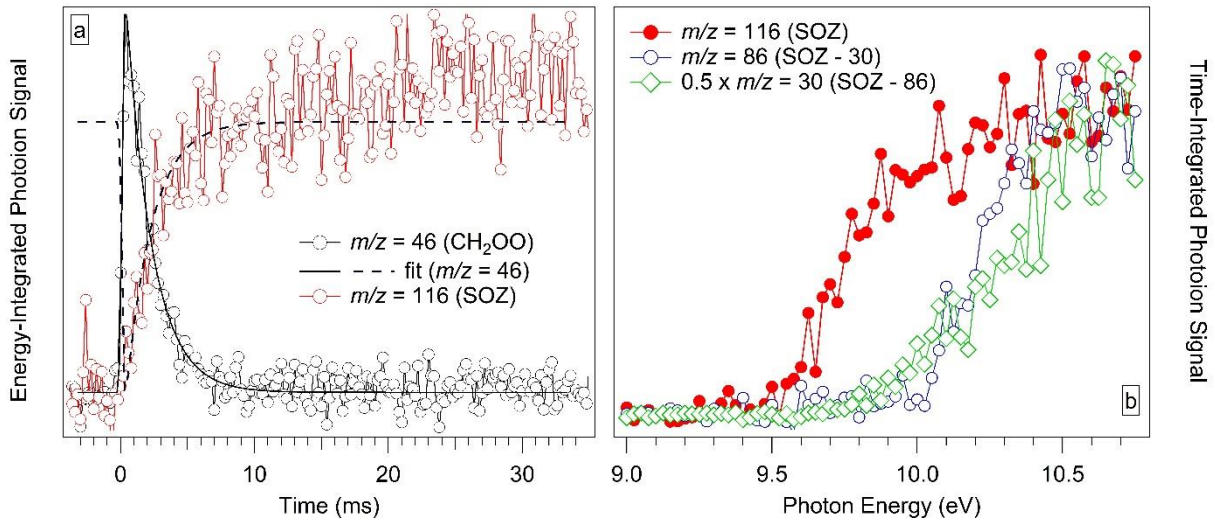

Figure 2. Experimental data from CH_2OO + $CH_2C(CH_3)CHO$ (methacrolein, MACR) reaction measurements at 4 Torr and about 300 K. **a**) Comparison of time behaviors of CH_2OO decay (signal at *m/z* = 46) with the formation of the CH_2OO-MACR adduct with parent *m/z* = 116. Also shown is a single-exponential fit to the CH_2OO signal decay trace. Time-resolved signals obtained by integration over photon energies from 9.0 – 10.75 eV. Signal intensities arbitrarily multiplied to facilitate comparison. **b**) Comparison of energy-resolved signals with potential origin from the CH_2OO-MACR adduct. Parent mass signal is at *m/z* = 116 and signal at *m/z* = 30 is suggested to originate from dissociative ionization of the CH_2OO-MACR adduct. Time-resolved signals of product formation are compared in Figure S3.

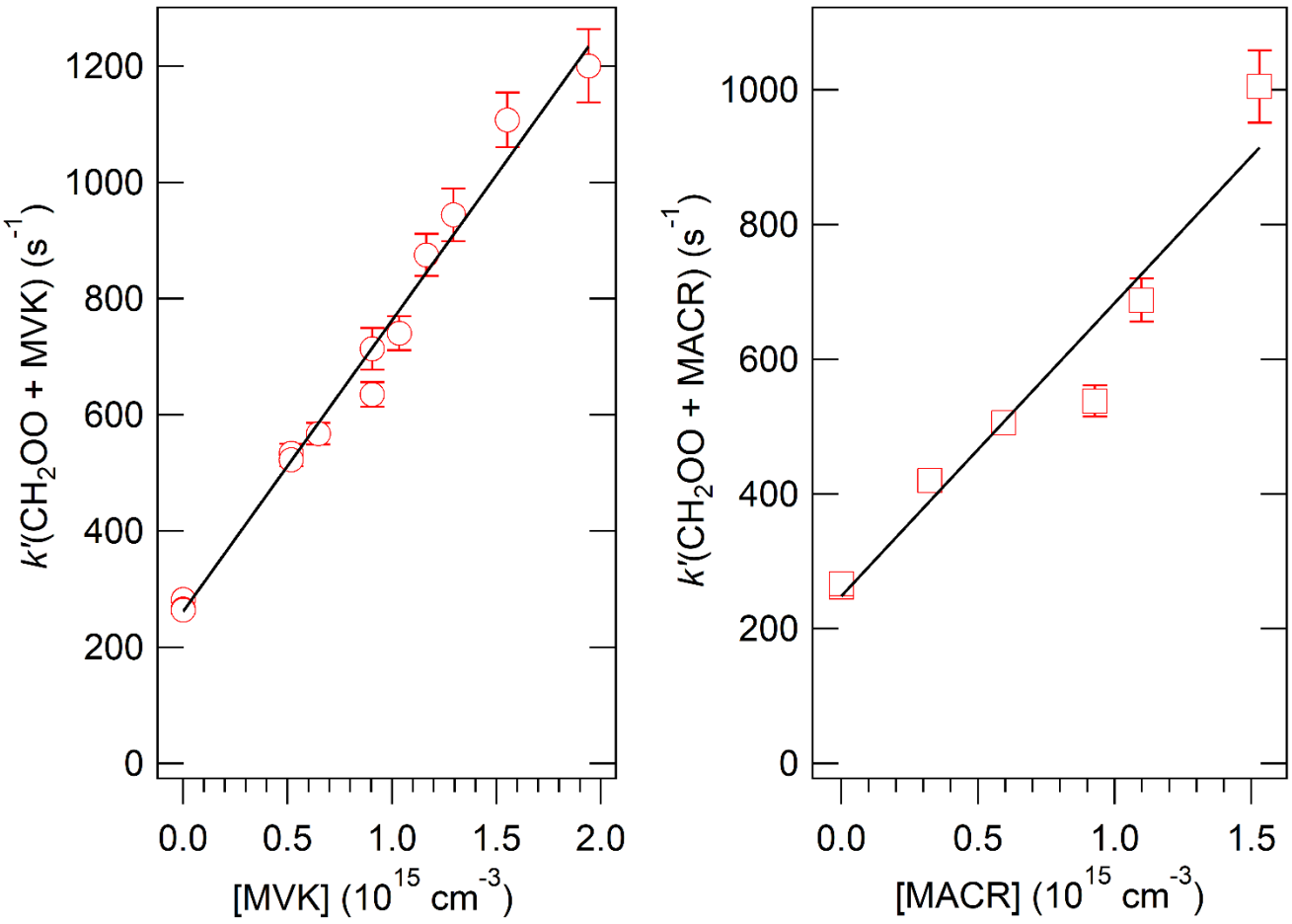

Figure 3. Bimolecular plots of CH_2OO + $CH_2C(CH_3)CHO$ (methacrolein, MACR) and CH_2OO + $CH_3C(O)CHCH_2$ (methyl vinyl ketone, MVK) reactions measured at 4 Torr and about 300 K. Linear fits to the data return $k(CH_2OO + MACR) = (4.4 \pm 1.0) \times 10^{-13}$ cm^3 s^{-1} and $k(CH_2OO + MVK) = (5.0 \pm 0.4) \times 10^{-13}$ cm^3 s^{-1} , where stated ± 2σ uncertainties are due to fitting uncertainties only.

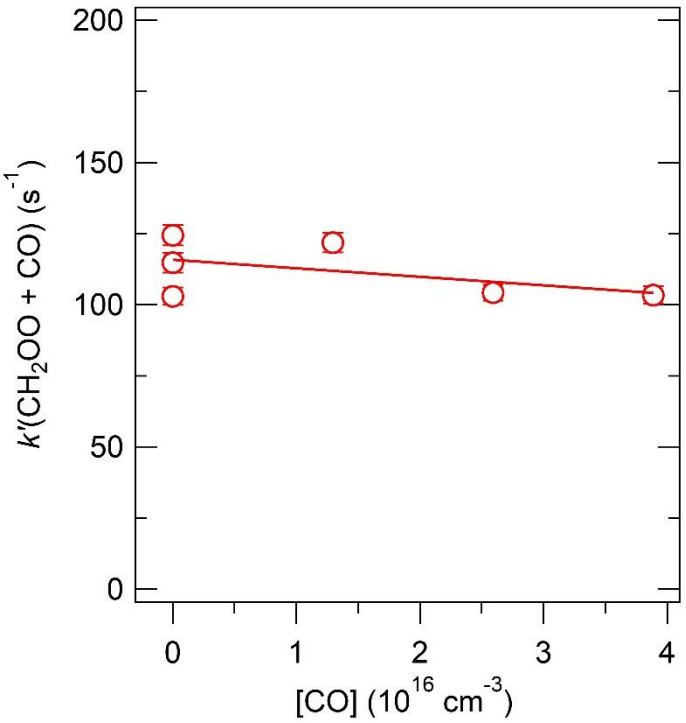

Figure 4. Bimolecular plot of CH_2OO decay rate at 4 Torr and 300 K temperature *versus* CO (carbon monoxide) concentration. A linear fit (solid line) to the data returns $k(CH_2OO + CO) = (-3.0 \pm 5.1) \times 10^{-16}$ ($\pm 2\sigma$ uncertainty) $cm^3\ s^{-1}$ from which an upper limit $k(CH_2OO + CO) < 2 \times 10^{-16}$ $cm^3\ s^{-1}$ is obtained.

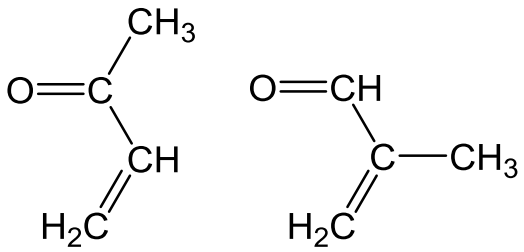

MVK **MACR**

Scheme 1. Structures of methyl vinyl ketone (MVK) and methacrolein (MACR).

(a) [1-(1,2-dioxolan-4-yl)ethan-1-one]: **AIE = 9.12 eV**

A

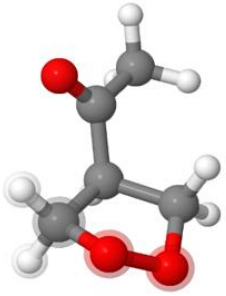

(b) [1-(1,2-dioxolan-3-yl)ethan-1-one]: **AIE = 9.04 eV**

B

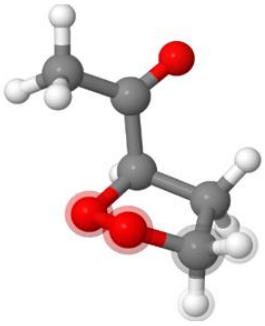

(c) [(*S*)-3-methyl-3-vinyl-1,2,4-trioxolane]: **AIE = 9.21 eV**

C

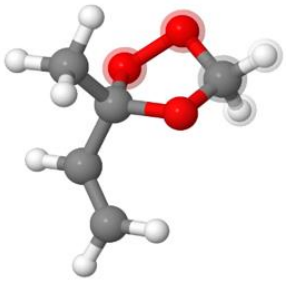

(d) [5-methyl-7*H*-1,2,4-trioxepine]: **AIE = 8.61 eV**

D

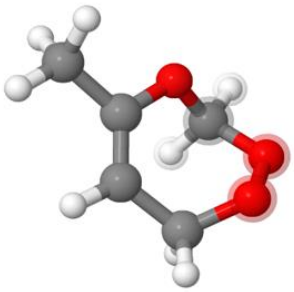

Scheme 2. Adduct structures from CH_2OO + MVK reaction and their calculated adiabatic ionization energies (AIE). The atoms which initially belonged to the CH_2OO are highlighted.

(e) [4-methyl-1,2-dioxolane-4-carbaldehyde]: **AIE = 9.25 eV**

E

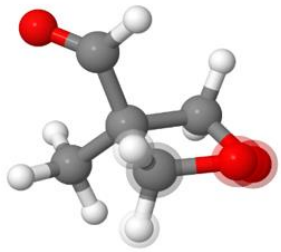

(f) [(*R*)-3-methyl-1,2-dioxolane-3-carbaldehyde]: **AIE = 9.29 eV**

F

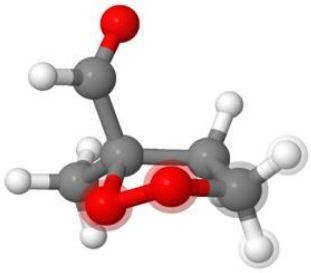

(g) [3-(prop-1-en-2-yl)-1,2,4-trioxolane]: **AIE = 9.45 eV**

G

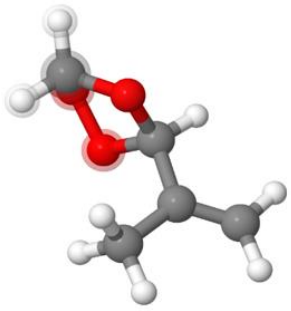

(h) [6-methyl-7*H*-1,2,4-trioxepine]: **AIE = 8.59 eV**

H

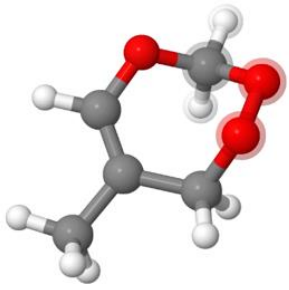

Scheme 3. Adduct structures from CH_2OO + MACR reaction and their calculated adiabatic ionization energies (AIE). The atoms which initially belonged to the CH_2OO are highlighted.

Table 1. Comparison of bimolecular reaction rate coefficients of CH_2OO with carbonyl and alkene compounds at about 300 K from the current and previous direct kinetics measurements.

Reactant	$k(CH_2OO + Reactant)$ / cm^3s^{-1}	Total pressure (Torr)	Reference
CF_3COCF_3	$(3.0 \pm 0.3)\times10^{-11}$	4	19
CH_3CHO	$(9.5 \pm 0.7)\times10^{-13}$	4	19
CH_3COCH_3	$(2.3 \pm 0.3)\times10^{-13}$	4	19
$CH_3COC_2H_3$	$(5.0 \pm 0.4)\times10^{-13}$	4	This work
$CH_2C(CH_3)CHO$	$(4.4 \pm 1.0)\times10^{-13}$	4	This work
CF_3CHCH_2	$< 1.75\times10^{-14}$	4	This work
CH_2CH_2	$(0.7 \pm 0.1)\times10^{-15}$	25	46
CH_3CHCH_2	$(1.8 \pm 0.3)\times10^{-15}$	25	46
$CH_2C(CH_3)CH_3$	$(1.4 \pm 0.3)\times10^{-15}$	25	46
$CH_2C(CH_3)CHCH_2$	$(1.5 \pm 0.1)\times10^{-15}$	15-100	47

Table 2. Calculated adiabatic ionization (AIE) energies of the SOZ compounds[a] in eV units.

Species	HF[b]	B3LYP	CC[c]	CBS[*]	**Combined**
A	8.13	8.73	9.24	8.89	**9.12**
B	8.65	8.61	9.43	9.04	**9.04**
C	*7.45*	8.64	9.31	9.07	**9.21**
D	8.20	8.22	8.66	8.57	**8.61**
E	8.40	8.99	9.37	9.01	**9.25**
F	8.27	8.76	9.43	9.07	**9.29**
G	*7.34*	8.87	9.64	9.11	**9.45**
H	8.27	8.17	8.64	8.53	**8.59**

[a] for full names please see Schemes 2 and 3.
[b] C−O bond dissociation at the HF/def2-TZVP level of theory caused strong deviation in the AIEs of compounds C and G (*cf. italic numbers*).
[c] DLPNO-CCSD(T)/CBS(TZ,QZ)

Table 3. Potential energies[a] at 0 K relative to CH_2OO + MVK/MACR (kcal mol^{-1}).

Species	vdW	TS	Adduct
A	-4.04	-1.08	-60.12
B	-4.78	-2.23	-62.88
C	-6.34	-4.06	-47.09
E	-- [b]	3.99	-57.25
F	-3.08	0.40	-61.47
G	-4.57	-3.63	-47.48

[a]DLPNO-CCSD(T)/CBS(TZ,QZ) level of theory

[b]Reaction has no pre-reaction van der Waals complex

5. References

1. D. Johnson and G. Marston, *Chem. Soc. Rev.*, 2008, **37**, 699-716.
2. R. Criegee, *Angew. Chem. Internat. Edit.*, 1975, **14**, 745-752.
3. T. L. Nguyen, H. Lee, D. A. Matthews, M. C. McCarthy and J. F. Stanton, *J. Phys. Chem. A*, 2015, **119**, 5524-5533.
4. L. Vereecken, D. R. Glowacki and M. J. Pilling, *Chem. Rev.*, 2015, **115**, 4063-4114.
5. O. Welz, J. D. Savee, D. L. Osborn, S. S. Vasu, C. J. Percival, D. E. Shallcross and C. A. Taatjes, *Science*, 2012, **335**, 204-207.
6. A. J. Eskola, D. Wojcik-Pastuszka, E. Ratajczak and R. S. Timonen, *Phys. Chem. Chem. Phys.*, 2006, **8**, 1416-1424
7. H. F. Huang, B. Rotavera, A. J. Eskola and C. A. Taatjes, *J. Phys. Chem. Lett.*, 2013, **4**, 3824-3824.
8. H. F. Huang, A. J. Eskola and C. A. Taatjes, *J. Phys. Chem. Lett.*, 2012, **3**, 3399-3403.
9. M. Sprengnether, K. L. Demerjian, N. M. Donahue and J. G. Anderson, *J. Geophys. Res.-Atmos.*, 2002, **107**, 13.
10. A. Miyoshi, S. Hatakeyama and N. Washida, *J. Geophys. Res.-Atmos.*, 1994, **99**, 18779-18787.
11. S. E. Paulson, R. C. Flagan and J. H. Seinfeld, *Int. J. Chem. Kinet.*, 1992, **24**, 79-101.
12. Y. J. Liu, I. Herdlinger-Blatt, K. A. McKinney and S. T. Martin, *Atmos. Chem. Phys.*, 2013, **13**, 5715-5730.
13. S. M. Aschmann and R. Atkinson, *Environ. Sci. Technol.*, 1994, **28**, 1539-1542.
14. F. Sauer, C. Schafer, P. Neeb, O. Horie and G. K. Moortgat, *Atmos. Environ.*, 1999, **33**, 229-241.
15. T. B. Nguyen, G. S. Tyndall, J. D. Crounse, A. P. Teng, K. H. Bates, R. H. Schwantes, M. M. Coggon, L. Zhang, P. Feiner, D. O. Milller, K. M. Skog, J. C. Rivera-Rios, M. Dorris, K. F. Olson, A. Koss, R. J. Wild, S. S. Brown, A. H. Goldstein, J. A. de Gouw, W. H. Brune, F. N. Keutsch, J. H. Seinfeld and P. O. Wennberg, *Phys. Chem. Chem. Phys.*, 2016, **18**, 10241-10254.
16. R. L. Kuczkowski, *Chem. Soc. Rev.*, 1992, **21**, 79-83.
17. P. Neeb, O. Horie and G. K. Moortgat, *Tetrahedron Lett.*, 1996, **37**, 9297-9300.
18. O. Horie, C. Schafer and G. K. Moortgat, *Int. J. Chem. Kinet.*, 1999, **31**, 261-269.
19. C. A. Taatjes, O. Welz, A. J. Eskola, J. D. Savee, D. L. Osborn, E. P. F. Lee, J. M. Dyke, D. W. K. Mok, D. E. Shallcross and C. J. Percival, *Phys. Chem. Chem. Phys.*, 2012, **14**, 10391-10400.
20. D. L. Osborn, P. Zou, H. Johnsen, C. C. Hayden, C. A. Taatjes, V. D. Knyazev, S. W. North, D. S. Peterka, M. Ahmed and S. R. Leone, *Rev. Sci. Instrum.*, 2008, **79**, 104103.
21. H. Keller-Rudek, G. K. Moortgat, R. Sander and R. Sorensen, *Earth Syst. Sci. Data*, 2013, **5**, 365-373.
22. J. M. Nicovich, K. D. Kreutter and P. H. Wine, *J. Chem. Phys.*, 1990, **92**, 3539-3544.
23. S. Grimme, S. Ehrlich, L. Goerigk, *J. Comput. Chem.*, 2011, **32**, 1456-1465.
24. C. Riplinger, P. Pinski, U. Becker, E. F. Valeev, F. Neese, *J. Chem. Phys.*, 2016, **144**, 024109.
25. M. Saitow, U. Becker, C. Riplinger, E. F. Valeev, F. Neese, *J. Chem. Phys.*, 2017, **146**, 164105.

26. A. Halkier, T. Helgaker, P. Jøorgensen, W. Klopper, H. Koch, J. Olsen and A. K. Wilson, *Chem. Phys. Lett.*, 1998, **286**, 243-252.
27. H. Kruse, M. Mladek, K. Gkionis, A. Hansen, S. Grimme, J. Sponer, *J. Chem. Theory Comput.*, 2015, **11**, 4972-4991.
28. F. Neese, *Wiley interdisciplinary Reviews - Computational Molecular Science*, 2012, **2**, 73-78.
29. S. Grimme, C. Bannwarth, P. Shushkov, *J. Chem. Theory Comput.*, 2017, **13**, 1989-2009.
30. J. C. Traeger, R. G. McLoughiin, A. J. C. Nicholson, *J. Am. Chem. Soc.*, 1982, **104**, 5318-5322.
31. J. C. Traeger, *J. Mass Spectrom.*, 1985, **20**, 223-227.
32. J. C. Traeger, *Int. J. Mass Spectrom. Ion Process.*, 1985, **66**, 271-282.
33. J. C. Traeger, D. J. McAdoo, *Int. J. Mass Spectrom. Ion Process.*, 1986, **68**, 35-48.
34. J. C. Traeger, *J. Phys. Chem.*, 1986, **90**, 4114-4118.
35. K. Watanabe, T. Nakayama, J. Motti, *J. Quant. Spectrosc. Radiat. Trans.*, 1962, **2**, 369-382.
36. E. Murad, M. G. Inghram, *J. Chem. Phys.*, 1964, **40**, 3263.
37. J.-P. Morizur, J. Mercier, M. Sarraf, *J. Mass Spectrom.*, 1982, **17**, 327-330.
38. K. V. Wood, J. W. Taylor, *Int. J. Mass Spectrom. Ion Process.*, 1979, **30**, 307-318.
39. D. A. Demeo, M. A. El-Sayed, *J. Chem. Phys.*, 1970, **52**, 2622.
40. E. P. L. Hunter, S. G. Lias, *J. Phys. Chem. Ref. Data*, 1998, **27**, 413.
41. J. C. Light, *J. Chem. Phys.*, 1964, **40**, 3221.
42. A. M. Dean, H.-H. Carstensen, *Comprehensive Chemical Kinetics*, 2007, **42**, 105-187.
43. H. Hippler, J. Troe, H. J. Wendelken, *J. Chem. Phys.*, 1983, **78**, 6709.
44. C. W. Gao, J. W. Allen, W. H. Green, R. H. West, *Comput. Phys. Comm.*, 2016, **203**, 212-225.
45. Y. Georgievskii, J. A. Miller, M. P. Burke, S. J. Klippenstein, *J. Phys. Chem. A*, 2013, **117**, 12146.
46. Z. J. Buras, R. M. I. Elsamra, A. Jalan, J. E. Middaugh and W. H. Green, *J. Phys. Chem. A*, 2014, **118**, 1997-2006.
47. Z. C. J. Decker, K. Au, L. Vereecken and L. Sheps, *Phys. Chem. Chem. Phys.*, 2017, **19**, 8541-8551.
48. M. S. Alam, M. Camredon, A. R. Rickard, T. Carr, K. P. Wyche, K. E. Hornsby, P. S. Monks and W. J. Bloss, *Phys. Chem. Chem. Phys.*, 2011, **13**, 11002-11015.
49. L. Vereecken, A. R. Rickard, M. J. Newland and W. J. Bloss, *Phys. Chem. Chem. Phys.*, 2015, **17**, 23847-23858.
50. R. Crehuet, J. M. Anglada, D. Cremer and J. M. Bofill, *J. Phys. Chem. A*, 2002, **106**, 3917-3929.
51. L. Vereecken, H. Harder and A. Novelli, *Phys. Chem. Chem. Phys.*, 2014, **16**, 4039-4049.
52. A. Jalan, J. W. Allen and W. H. Green, *Phys. Chem. Chem. Phys.*, 2013, **15**, 16841-16852.